嗜中性球在輻射誘發的抗腫瘤免疫反應中的關鍵作用：用G-CSF 增強

# Key role for neutrophils in radiation-induced antitumor immune responses: Potentiation with G-CSF

Tsuguhide Takeshima[a], Laurentiu M. Pop[b], Aaron Laine[a], Puneeth Iyengar[a], Ellen S. Vitetta[b,c,1], and Raquibul Hannan[a,1]

[a]Department of Radiation Oncology, University of Texas Southwestern Medical Center, Dallas, TX 75390; [b]Department of Immunology, University of Texas Southwestern Medical Center, Dallas, TX 75390; and [c]Department of Microbiology, University of Texas Southwestern Medical Center, Dallas, TX 75390

Contributed by Ellen S. Vitetta, August 11, 2016 (sent for review April 15, 2016; reviewed by Jadwiga Jablonska and Laurence Zitvogel)

**Radiation therapy (RT), a major modality for treating localized tumors, can induce tumor regression outside the radiation field through an abscopal effect that is thought to involve the immune system. Our studies were designed to understand the early immunological effects of RT in the tumor microenvironment using several syngeneic mouse tumor models. We observed that RT induced sterile inflammation with a rapid and transient infiltration of $CD11b^{+}Gr\text{-}1^{high+}$ neutrophils into the tumors. RT-recruited tumor-associated neutrophils (RT-Ns) exhibited an increased production of reactive oxygen species and induced apoptosis of tumor cells. Tumor infiltration of RT-Ns resulted in sterile inflammation and, eventually, the activation of tumor-specific cytotoxic T cells, their recruitment into the tumor site, and tumor regression. Finally, the concurrent administration of granulocyte colony-stimulating factor (G-CSF) enhanced RT-mediated antitumor activity by activating RT-Ns. Our results suggest that the combination of RT and G-CSF should be further evaluated in preclinical and clinical settings.**

radiation therapy | tumor-associated neutrophils | G-CSF

Radiation therapy (RT) is one of the three core modalities for the treatment of cancer, although tumor recurrence is observed even with high doses of fractionated stereotactic RT (1). Recent studies have shown that RT-induced tumor cell death is "immunogenic" and that RT generates antitumor immune responses, including cytotoxic T lymphocytes (CTLs) (2), the main effectors against tumor cells (3).

Tumor-associated neutrophils (TANs) can have both anti- and protumor effects (4–6). As in the case of tumor-associated macrophages, where alternative polarization pathways (M1 versus M2) are involved, a paradigm of antitumor "N1 neutrophils" versus protumor "N2 neutrophils" has been proposed using mouse tumor models (7) in which TGF-β blocked the switch from the "N2" to the "N1" antitumorigenic phenotype. It has been demonstrated that tumors grow faster in the absence of endogenous IFN-β because antitumor N1 TANs are not induced (5, 8). In addition, neovascularization increased numbers of infiltrating N2 TANs expressing higher levels of CXCR4 and vascular endothelial growth factor (VEGF) were observed (5, 8). In a clinical study conducted in surgically resected patients with early-stage lung cancer, it has been demonstrated that TANs are not immunosuppressive but, instead, stimulate T-cell responses (9). Thus, the role of TANs in tumor immunology and the conditions triggering anti- and protumor polarization are still not fully understood.

Sterile inflammation occurs in the absence of pathogens following tissue damage (10, 11). The hallmark of sterile inflammation is the rapid infiltration of neutrophils, as is also observed in the spleen, thymus, and gut after whole-body ionizing radiation in mice (12–14). Inflammatory responses, known as damage-associated molecular patterns (DAMPs), which are released from dying cells, are initiated by endogenous molecules (10, 15, 16). DAMPs activate sentinel cells to release proinflammatory mediators (e.g., IL-1β, TNF) and neutrophil-active chemoattractants [e.g., MIP-2, SDF-1, RANTES, chemokine receptor CXCR2 ligand (KC), IL-8, LTB4] (11, 17), initiating the recruitment of neutrophils into the tissue.

This study reports neutrophil-mediated sterile inflammation as a result of RT of tumors. We demonstrate a rapid and transient infiltration of TANs after local irradiation [RT-recruited TANs (RT-Ns)]. RT alone or in combination with granulocyte colony-stimulating factor (G-CSF) induces the polarization of antitumor N1 (RT-Ns), which produce reactive oxygen species (ROS).

## Results

**$CD11b^{+}Gr\text{-}1^{high+}$ Neutrophils Are Increased in the Tumor Microenvironment 24 h After Focal Tumor Irradiation.** Because $CD11b^{+}Gr\text{-}1^{high+}$ cells in tumor tissue were identified as neutrophils (TANs) (18), we isolated them from syngeneic tumor grafts of both irradiated (15 Gy) and nonirradiated tumors of RM-9–bearing C57BL/6 mice using flow cytometry, and observed a neutrophil-like morphology (Fig. 1*A*).

To examine the infiltration of TANs after focal irradiation, flow cytometric analysis was performed on cells obtained from syngeneic tumor grafts of RM-9–bearing C57BL/6, 4T1-bearing BALB/c, and EG7-bearing C57BL/6 mice between 0 and 96 h after 15 Gy, 15 Gy, and 1.3 Gy of focused irradiation, respectively. Differences in optimal radiation doses between RM-9, 4T1, and EG7 tumors were due to their varying radiosensitivities (Fig. S1).

An increase in $CD11b^{+}Gr\text{-}1^{high+}$ cells infiltrating RM-9 (from 18.4 to 26.7%), 4T1 (from 26.1 to 42.7%), and EG7 (from 4.9 to 9.0%) tumors was observed 24 h after tumor irradiation (Fig. 1*A* and Fig. S2 *A* and *B*). In all tumor models, the TANs within the lymphocyte and granulocyte populations began to increase at 12 h after an initial transient decrease at 6 h, peaked at 24 h, and steadily declined thereafter (Fig. 1*B* and Fig. S2 *A* and *B*). Although the initial decrease is likely due to radiation, the results

### Significance

**The role of tumor-associated neutrophils (TANs) in cancer progression versus regression remains controversial. TANs are known to have dichotomous antitumor (N1) and protumor (N2) phenotypes depending on the tumor microenvironment. Past studies have demonstrated that TANs are polarized from an N2 to an N1 phenotype in the absence of TGF-β; N1 TANs are not induced in the absence of IFN-β. Our study demonstrates that radiation therapy (RT) and, especially, the combination of RT and granulocyte colony-stimulating factor (G-CSF) induces the polarization of N1 TANs [RT-recruited TANs (RT-Ns)]. Reactive oxygen species produced by RT-Ns damage tumor tissues in a manner analogous to the manner in which neutrophils affect damaged normal tissues. Our studies suggest that enhancing the activity of TANs during RT improves its antitumor activity.**

Author contributions: T.T., E.S.V., and R.H. designed research; T.T. and L.M.P. performed research; R.H. contributed new reagents/analytic tools; T.T. and R.H. analyzed data; and T.T., L.M.P., A.L., P.I., E.S.V., and R.H. wrote the paper.

Reviewers: J.J., University Hospital Essen; and L.Z., Institut Gustave Roussy-France.

The authors declare no conflict of interest.

Freely available online through the PNAS open access option.

[1]To whom correspondence may be addressed. Email: raquibul.hannan@utsouthwestern.edu or ellen.vitetta@utsouthwestern.edu.

This article contains supporting information online at www.pnas.org/lookup/suppl/doi:10.1073/pnas.1613187113/-/DCSupplemental.

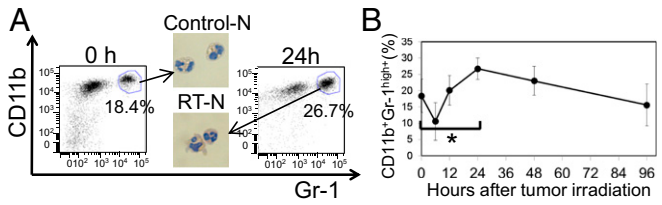


**Fig. 1.** TANs ($CD11b^+Gr\text{-}1^+$ cells) in the gated population of lymphocytes and granulocytes increased 24 h after tumor irradiation. RM-9–bearing C57BL/6 mice were irradiated with 15 Gy. Morphology and sorting of purified $CD11b^+Gr\text{-}1^{high+}$ cells at 24 h (*A*) and changes over time (*B*) in the percentage of TANs within the lymphocytes and granulocytes of the tumor tissue following irradiation of RM-9 are shown. Harvested tumor tissues were analyzed by flow cytometry. Similar results were obtained from three independent experiments. Analysis of differences was performed by the Mann–Whitney *U* test (*$P < 0.05$).

demonstrate that this transient decrease is followed by an early RT-mediated infiltration of TANs.

**RT-Ns Inhibit Tumor Growth Following Focal Irradiation.** Neutrophil-depleted mice were used to ascertain the effect of TANs recruited into the tumors following RT (RT-Ns). To deplete neutrophils, mice were treated with an anti–Ly-6G monoclonal antibody [mAb; clone 1A8 as previously described (19)]. We previously used the anti–Ly-6G mAb and confirmed that $CD11b^+Ly\text{-}6G^+$ and $CD11b^+Gr\text{-}1^{high+}$ cells (TANs) are equivalent (Fig. S3). We also observed that a single intraperitoneal (i.p.) injection of anti–Ly-6G mAb induced the complete depletion of TANs (Fig. S4) for up to 7 d (Fig. S5).

We next evaluated the antitumor effect of RT in neutrophil-depleted mice using the RM-9, 4T1, and EG7 tumor models after 15 Gy, 15 Gy, and 1.3 Gy of focused irradiation, respectively. RT and antibody therapy were as follows: (*i*) rat isotype IgG control, (*ii*) anti–Ly-6G mAb, (*iii*) RT + rat isotype IgG control, and (*iv*) RT + anti–Ly-6G mAb. Antibodies were injected 1 d before RT to ensure neutrophil depletion during RT. As shown in Fig. 2 and Fig. S6 *A* and *B*, no difference in growth was observed in the tumors in the absence of RT. However, a significant increase in tumor growth was observed following neutrophil depletion compared to tumor growth after RT. These observations suggest that RT-Ns play an important role in the antitumor activity of RT.

**ROS Produced by RT-Ns Are Essential for the Antitumor Activity of RT.** We next examined the differences between RT-Ns and $CD11b^+Gr\text{-}1^{high+}$ neutrophils in nonirradiated tumors (Control-Ns) using RM-9– and 4T1 tumor-bearing mice. To evaluate ROS production, TANs in cell suspensions from tumor homogenates were stimulated with *N*-formyl-L-methionyl-L-leucyl-phenylalanine (formyl peptide receptor 1 ligand) and the gated $CD11b^+Gr\text{-}1^{high+}$ cells were analyzed by flow cytometry. We observed a significant increase in ROS production by RT-Ns compared with ROS production by Control-Ns in both tumor models (Fig. 3*A* and Fig. S7). These results demonstrate that the RT-Ns were specifically activated.

To determine whether the observed antitumor effect of RT-Ns was ROS-mediated, we used the NADPH oxidase inhibitor diphenyleneiodonium (DPI) to inhibit ROS production (20, 21). DPI was administered i.p. to mice 5 min after tumor irradiation when the effect of the RT-induced ROS effect was complete (the lifetime of ROS in a cell is a few nanoseconds) (22, 23).

Local RT of RM-9 tumor-bearing mice caused significant inhibition of tumor growth compared with untreated mice (Fig. 3*B*). However, administration of DPI into tumor-bearing mice reversed the inhibition of RT-mediated inhibition of tumor growth as effectively as the anti–Ly-6G mAb. These results demonstrate that the enhancement of RT antitumor activity by RT-Ns is ROS-mediated.

**RT-Ns Induce Oxidative Damage and Apoptosis of Tumor Cells.** ROS react with the plasma membrane, functional proteins, and nucleic acids, leading to oxidative damage and cell death (24). We assessed oxidative damage and apoptosis in RM-9 tumor tissues by immunohistochemical analysis using mAbs against the oxidative stress markers 8-hydroxydeoxyguanosine (8-OHdG) and 4-hydroxy-2-nonenal (4-HNE) and the flow cytometric analysis of terminal deoxynucleotidyl transferase dUTP nick end labeling (TUNEL) assay (24).

As shown in Fig. 4 *A*–*D*, an increase in $8\text{-}OHdG^+$ and $4\text{-}HNE^+$ cells, which are surrogates for oxidative damage, was clearly observed in the tumors from irradiated, but not nonirradiated, mice (8-OHdG: from 4.5 to 61.9%, 4-HNE: from 35.8 to 79.1%). However, compared with mice treated with the isotype-matched control, cells with oxidative damage were markedly decreased in the tumors from irradiated mice treated with the anti–Ly-6G mAb before RT (8-OHdG: 15.0%, 4-HNE: 59.2%) (Fig. 4 *A*–*D*).

A similar trend was found in the TUNEL assay, with a significant increase of apoptotic cells in irradiated tumors compared with nonirradiated tumors. This phenomenon was abolished when the irradiated mice were neutrophil-depleted (Fig. 4 *E* and *F*). The observed trends in oxidative damage and apoptosis are consistent with the difference in tumor size between normal and neutrophil-depleted mice (Fig. 2*A*). Taken together, these results suggest that the ROS produced by RT-Ns are likely responsible for oxidative damage and apoptosis of tumors, leading to the enhanced therapeutic effect of RT.

**Cytokine and Chemokine Levels in Tumors Are Increased After Irradiation.** To investigate the mechanism involved in the recruitment of neutrophils into tumor tissue following irradiation, changes in chemokines and cytokines involved in the recruitment and activation of neutrophils were analyzed in RM-9 tumors. Tumors were harvested at various time points (0, 6, 12, 24, 48, and 96 h) after focal irradiation with 15 Gy. Tumor tissue lysates were analyzed using a cytokine array kit. Although significant increases in G-CSF, IL-1β, and KC levels were observed in the

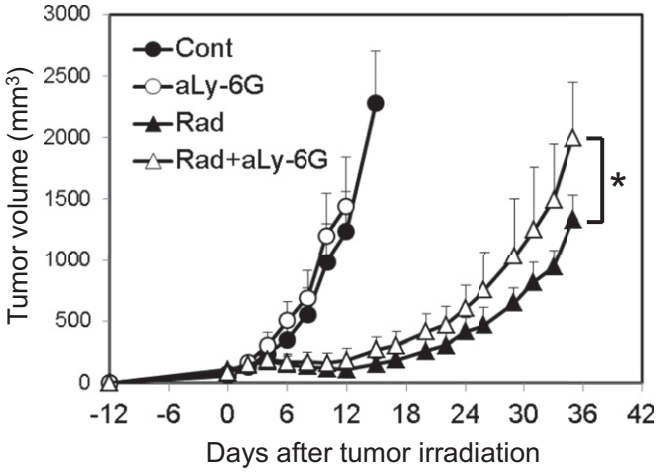


**Fig. 2.** RT-Ns are involved in the therapeutic response to RT. RM-9–bearing C57BL/6 mice were irradiated (▲ and △) with 15 Gy or nonirradiated (● and ○) and treated with anti–Ly-6G (aLy-6G) mAb (△ and ○) or isotype control (▲ and ●). Each point includes an average of five mice per experimental group; bars represent SD. Similar results were obtained from three independent experiments. Analysis of differences was performed by two-way ANOVA (*$P < 0.05$). Cont, control; Rad, irradiation.

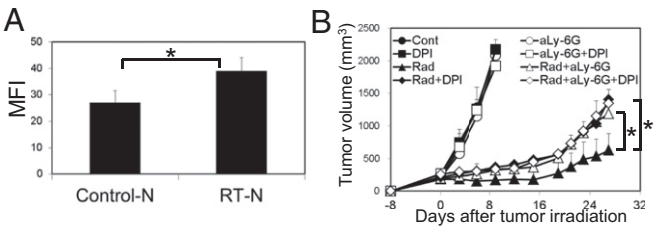


**Fig. 3.** Production of ROS from RT-Ns is higher than in nonirradiated tumors (Control-Ns); ROS depletion attenuates the antitumor effect of RT. (*A*) ROS production in TANs from RM-9–bearing C57BL/6. TANs ($CD11b^{+}Gr\text{-}1^{high+}$ cells) were analyzed by flow cytometry using cells prepared from tumor tissues. (*B*) RM-9–bearing C57BL/6 mice were irradiated (▲, △, and ■) with 15 Gy or unirradiated (●, ○, and □) and treated with anti–Ly-6G mAb (○ and △), isotype control (●, ▲, □, and ■) or DPI (□ and ■). Similar results were obtained from two independent experiments. Analysis of differences was performed by two-way ANOVA (*$P < 0.05$).

irradiated tumor within 48 h (Fig. 5*A*), only the G-CSF increase was confirmed by ELISA (Fig. 5*B* and Fig. S8 *A* and *B*). These results suggest that higher levels of G-CSF in the tumor contribute to the infiltration of RT-Ns.

**The Concurrent Use of RT and G-CSF Increases ROS Production by RT-Ns and Enhances the Antitumor Activity of RT.** We next hypothesized that the exogenous administration of G-CSF should further increase the production of ROS by activating neutrophils in tumors, hence enhancing the efficacy of RT. To test this hypothesis, we evaluated ROS production by RT-Ns after G-CSF administration. Tumor tissues were obtained 24 h after irradiation with 15 Gy and injection of G-CSF. $CD11b^{+}Gr\text{-}1^{high+}$ cells were assessed by flow cytometry following staining with dihydrorhodamine 123 as previously described (25). ROS production by RT-Ns [mean fluorescence intensity (MFI) of 57 and 74] was enhanced by RT and further increased by G-CSF (MFI of 91) (Fig. 6*A*).

To analyze the effects of RT combined with G-CSF, oxidative damage and apoptosis were assessed in tumor tissue by flow cytometric analysis with TUNEL (Fig. 4). The number of $8\text{-OHdG}^{+}$ and $4\text{-HNE}^{+}$ cells was increased in tumors from mice treated with both RT and G-CSF compared with mice treated with RT alone (8-OHdG: from 63.6 to 81.5%, 4-HNE: from 79.3 to 89.2%) (Fig. 6 *B*–*E*). No significant difference ($P > 0.05$) was noted using 8-OHdG, but a difference ($P < 0.05$) in the percentage of $4\text{-HNE}^{+}$ cells was observed between mice treated with G-CSF alone and untreated mice (8-OHdG: 27.7% and 27.9%, 4-HNE: 27.9% and 48.0%) (Fig. 6 *B*–*E*). In addition, $TUNEL^{+}$ cells were increased in tumors from mice receiving combined treatment compared with those mice treated with RT alone (from 16.0 to 25.4%). Nevertheless, the difference between the mice treated with G-CSF alone and untreated mice (8.9% and 4.5%) was not statistically significant ($P > 0.05$). This result confirms that the observed increase in the efficacy of RT as a result of concurrent administration of G-CSF is mediated by increased oxidative damage and apoptosis.

**Concurrent G-CSF and RT Lead to Decreased Tumor Growth Because of Higher ROS Production by RT-Ns.** The efficacy of RT combined with G-CSF was evaluated in RM-9, 4T1, and EG7 tumor-bearing mice. Tumor growth was inhibited significantly in groups receiving combination therapy compared with the control mice receiving RT alone (Fig. 7*A* and Fig. S9 *A* and *B*). The results suggest that the antitumor activity of RT can be augmented by concurrent administration of G-CSF.

We next investigated the contribution of ROS and $CD8^{+}$ cells to the therapeutic effect of RT and G-CSF. We also determined whether the RT-N–induced therapeutic effect could be abolished by depleting $CD8^{+}$ cells using an anti-CD8 mAb. RM-9 tumor grafts grew faster when neutrophils, $CD8^{+}$ cells, and ROS were depleted by anti–Ly-6G mAb, anti-CD8 mAb, and DPI, respectively (Fig. 7*B*).

These results demonstrate that combining RT with G-CSF therapy is likely mediated by ROS produced from G-CSF–stimulated RT-Ns. Furthermore, this increased therapeutic efficacy requires $CD8^{+}$ cells. Therefore, increased ROS-mediated tumor death likely leads to more robust presentation of tumor antigens, and eventually to the downstream generation of tumor-specific CTLs.

**G-CSF Enhances the RT-Mediated Production of Tumor-Specific CTLs.** Tumor RT has been implicated in initiating antigen presentation by dying cells, priming tumor-specific CTLs, and inducing an adaptive antitumor immune response enhancing therapeutic efficacy (26–29). We hypothesized that the increased antitumor efficacy of RT observed during the coadministration of G-CSF might be linked to an improved RT-mediated adaptive tumor-specific immune response. We therefore investigated whether tumor-specific CTLs were increased by G-CSF–mediated ROS production by RT-Ns. To evaluate tumor-specific CTL production, we quantified ovalbumin (OVA)-$tetramer^{+}CD8^{+}$ cells in an EG7 tumor model (EL4 transduced to express OVA) by flow cytometry.

Lymphocytes isolated from the draining lymph nodes (DLNs) and tumor tissues were evaluated for the presence of an OVA-specific CTL population by staining cells with the OVA/$H\text{-}2^{Kb}$ tetramer. The frequencies of OVA-$tetramer^{+}CD8^{+}$ cells were

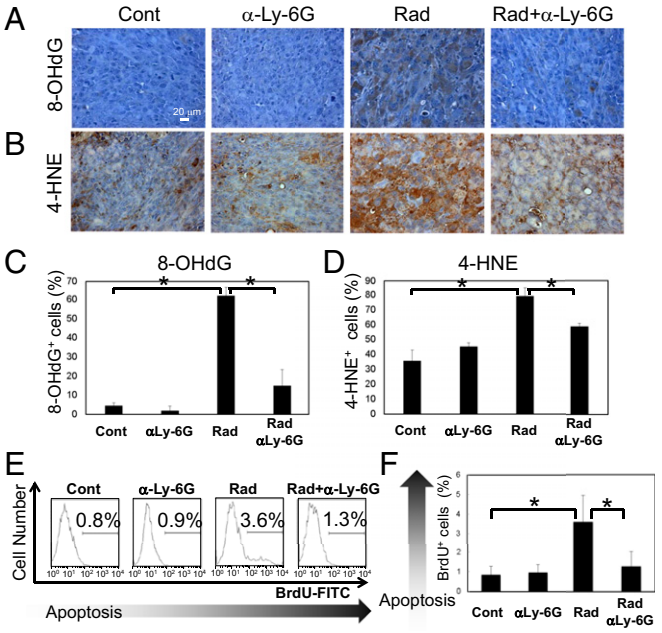


**Fig. 4.** RT-Ns damage tumor tissues and induce apoptosis. Immunohistochemical analysis with mAbs against 8-OHdG (*A*) and 4-HNE (*B*) to detect DNA damage and oxidative stress in RM-9 tumor tissues, respectively, is shown. (Original magnification, 400×.) (Scale bar, 20 μm.) Quantitative assessment of cells positive for 8-OHdG (*C*) and 4-HNE (*D*) [$n = 4$ per group; 4 high-power fields (HPFs) were counted per sample] is shown. (*E* and *F*) Detection of apoptotic cells in RM-9 tumor tissues by TUNEL using flow cytometric analysis. RM-9 tumor tissues were obtained 4 d after irradiation. To deplete neutrophils, RM-9–bearing mice were injected i.p. with anti–Ly-6G mAb 1 d before irradiation. Similar results were obtained from two independent experiments. Analysis of differences was performed by the Mann–Whitney *U* test (*$P < 0.05$).

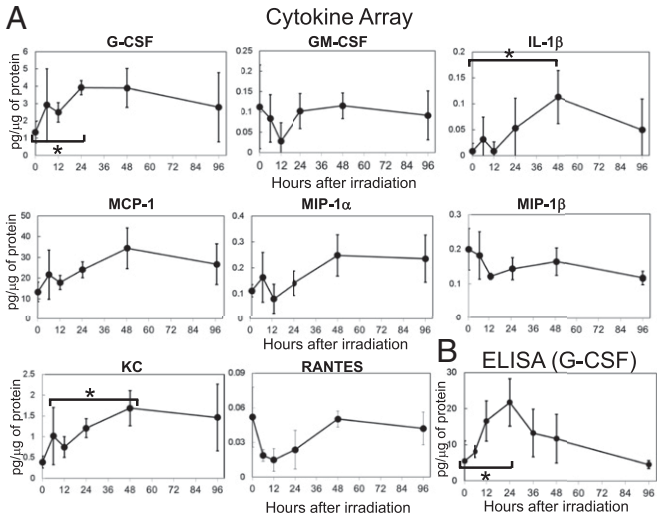


**Fig. 5.** Cytokine profile in tumor tissue after irradiation. G-CSF levels increased 24 h after irradiation. (*A*) RM-9 tumor lysates were analyzed by a Bio-Plex Pro Mouse Cytokine 23-plex Assay ($n = 4$). (*B*) RM-9 tumor lysates were analyzed by a G-CSF ELISA kit ($n = 5$). RM-9 tumors were harvested at 0, 6, 12, 24, 48, and 96 h after irradiation. Similar results were obtained from two independent experiments. Analysis of differences was performed by the Mann–Whitney *U* test (*$P < 0.05$).

elevated in DLNs (from 0.2 to 0.8%) and tumor tissues (from 0.2 to 1.3%) of EG7-bearing mice treated with RT compared with the frequencies of untreated mice (Fig. 8 *A* and *B*). The frequency of the OVA-tetramer$^+$CD8$^+$ cells was further elevated in DLNs (2.7%) and tumor tissues (3.7%) of mice receiving concurrent administration of RT and G-CSF compared with mice treated with either RT or G-CSF alone.

We next investigated the role of RT-Ns and ROS in mice treated with both G-CSF and RT. The frequencies of the OVA-tetramer$^+$CD8$^+$ cells were amplified in DLNs (from 0.6 to 1.3%) and tumor tissues (from 2.3 to 6.8%) after combination therapy when compared with the control and RT-alone groups (Fig. 8 *C* and *D*). In addition, depletion of RT-Ns or ROS led to a decrease in OVA-tetramer$^+$CD8$^+$ cells in DLNs (0.8% or 0.4%) and tumors (4.2% or 2.8%) after combination therapy (Fig. 8 *C* and *D*).

These findings suggest that G-CSF can amplify the adaptive tumor-specific immune response initiated by RT; this amplification may be mediated by ROS production by the G-CSF–stimulated RT-Ns.

## Discussion

The major findings that emerge from our study are as follows: (*i*) Focal tumor RT leads to the early recruitment of RT-Ns; (*ii*) RT-Ns increase their production of ROS compared with Control-Ns, which originally reside in the tumor, and this increased ROS leads to oxidative damage, apoptosis of tumor cells, and tumor shrinkage; and (*iii*) G-CSF can activate RT-Ns leading to increased ROS-mediated damage, tumor cell apoptosis, and the subsequent activation of tumor-specific CTLs.

RT-Ns may have characteristics similar to those observed in normal tissues during sterile inflammation. This study demonstrated that RT leads to the transient (within 24 h) infiltration of neutrophils into the tumor. Although the mechanisms leading to neutrophilic infiltration have not been defined, it is likely that the DAMPs released by tumor or stromal cells after RT may be responsible for the early recruitment of RT-Ns (2, 30, 31). In accordance with this finding, other studies have reported the transient infiltration of neutrophils into normal tissues within 24 h after irradiation (12, 13). The ROS produced by neutrophils responsible for tissue damage during sterile inflammation have also been observed in mouse models of ischemia (24).

RT-Ns, as demonstrated here, are an example of the antitumor N1 behavior of TANs and confirm previous observation that after TGF-β blockade, neutrophils acquire an antitumor phenotype (i.e., protumor N2 cells become antitumor N1 cells) (7). Fridlender et al. (7) also showed that the antitumor activity of N1 TANs is mediated by ROS/$H_2O_2$. It has been reported that a lack of IFN-β leads to the accumulation of increased protumor N2 neutrophils in tumors, resulting in the promotion of tumor growth as previously reported (8, 32). Conversely, increased IFN-β induces the antitumor N1 phenotype (33). It has also been demonstrated that TANs in early-stage human lung cancer are more cytotoxic to tumor cells (9) compared with TANs in larger and more advanced tumors (34).

The origins of RT-Ns may differ from the origins of antitumor N1s reported by Fridlender et al. (7) (Fig. S10). The effect of RT-Ns may therefore be secondary to recruitment rather than a phenotypic polarization of TANs.

G-CSF up-regulates the expression of antitumor neutrophil markers, such as ICAM1 and TNF-α, and promotes the formation of neutrophil extracellular traps (NETs) (33, 35, 36). As

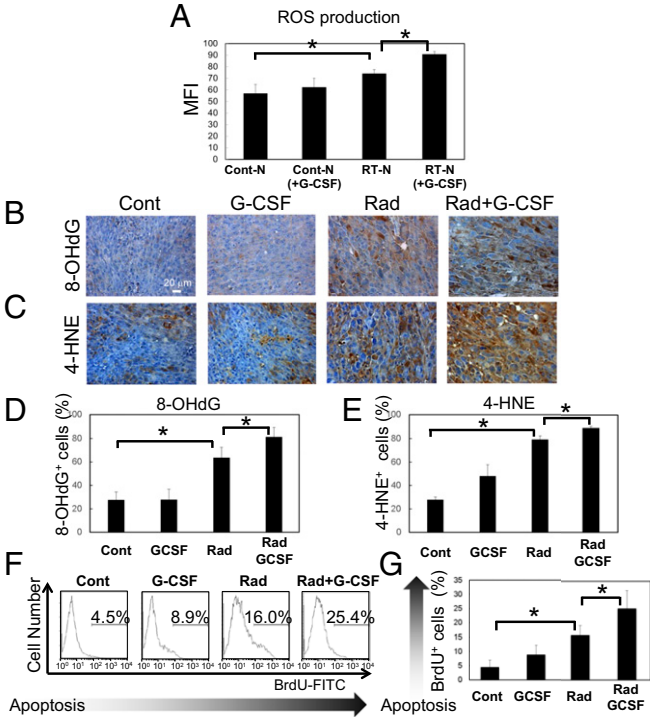


**Fig. 6.** G-CSF combined with RT causes tumor destruction by increasing cellular oxidative stress and accelerating apoptosis. G-CSF was injected s.c. into RM-9–bearing mice on the same day as irradiation treatment, and then for 4 consecutive days. (*A*) ROS production by RT-Ns treated with G-CSF in RM-9–bearing mice. Tumor tissues were obtained 1 d after irradiation and administration of G-CSF. TANs (CD11b$^+$Gr-1$^{high+}$ cells) were analyzed by flow cytometry, and cells were prepared from tumor tissues. Immunohistochemical analysis with mAbs against 8-OHdG (*B*) and 4-HNE (*C*) detected DNA damage and oxidative stress in tumor tissues, respectively. Tumor tissues were obtained 4 d after irradiation. (Original magnification, 400×). (Scale bar, 20 μm.) Quantitative assessment of cells positive for 8-OHdG (*D*) and 4-HNE (*E*) ($n = 4$ per group; 4 HPFs were counted per sample) is shown. (*F* and *G*) Detection of apoptotic cells by the TUNEL method using flow cytometric analysis. Tumor tissues were obtained 4 d after irradiation. Each point is the mean of five mice in each experimental group; similar results were obtained from two independent experiments. Analysis of differences was performed by the Mann–Whitney *U* test (*$P < 0.05$).

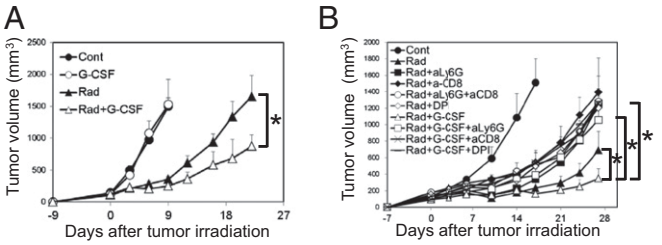


**Fig. 7.** G-CSF augments the antitumor RT-N response in tumor-bearing mice. G-CSF was injected s.c. for 4 consecutive days, starting on the day of RT administration for RM-9–, 4T1-, and EG7-bearing mice. (*A*) RM-9–bearing mice were irradiated (▲ and △) with 15 Gy or nonirradiated (● and ○) and treated with s.c. injection of G-CSF (△ and ○) or PBS (▲ and ●). (*B*) RM-9–bearing mice were irradiated with 15 Gy either alone or in combination with anti–Ly-6G mAb, anti-CD8 mAb, DPI, and G-CSF. Similar results were obtained from three independent experiments. Analysis of differences was performed by two-way ANOVA (*$P < 0.05$).

expected, the concurrent administration of G-CSF and RT resulted in increased antitumor activity. Even though G-CSF only marginally increased ROS production by RT-Ns, this effect, combined with the enhanced antitumor CTLs, may have contributed to the observed reduction of tumor volume.

The clinical anticancer effects of G-CSF are currently unclear. Although some clinical trials have demonstrated promising effects (37, 38), others have described potential adverse effects (39–41). Additionally, G-CSF can either activate or increase the recruitment and activity of protumor neutrophils and other myeloid-derived suppressor cells (MDSCs), enhancing tumor growth via angiogenesis by up-regulating VEGF (42), or in combination with an anti-VEGF antibody (43), paclitaxel (40), and γ-irradiation (44). These contrasting results may be related to the temporal appearance of different neutrophils versus other MDSCs in tumors depending on the therapeutic regimen used. For example, Kim et al. (44) delivered 2 Gy to mice daily for 5 d, with seven injections of G-CSF for 6 d, whereas the mice in our study only received a single 15-Gy RT dose with four injections of G-CSF for 3 d. This difference in RT delivery is supported by clinical data indicating a protumor effect by G-CSF with conventional fractionated RT (39). In contrast, an antitumor effect was observed when RT was delivered in limited fractions (45). This observation suggests that early influx of RT-N may not occur after delivering repeated doses of RT, highlighting the importance of developing treatment regimens to amplify the infiltration of TANs immediately after RT.

Although many studies have shown that RT induces tumor-specific immune responses (26–29, 46), our study demonstrates that the generation of tumor-specific CTLs ($CD8^+$OVA-$tetramer^+$ cells) is increased by the combination of RT and G-CSF. In addition, we demonstrated that ROS produced by G-CSF–stimulated RT-Ns are involved in the amplification of tumor-specific CTLs. Therefore, G-CSF might be essential in initiating an RT-induced adaptive immune response. Although it is unclear whether the G-CSF–mediated increase in the antitumor CTL response is mediated by RT-Ns, we presume that the dead cells induced by ROS-producing RT-Ns stimulate tumor immune responses by inducing sterile infiltration in which dendritic cells become more effective (47). Singhal et al. (48) reported that a subset of TANs exhibited characteristics of both neutrophils and antigen-presenting cells in early-stage human lung cancer. Lim et al. (49) recently showed that the chemokine CXCL12 produced by neutrophils provides chemotactic haptotactic signals for the efficient recruitment of CTLs into sites of infection. Neutrophils can guide influenza-specific CTLs into the airways. Therefore, RT-Ns likely play a critical role in the amplification of G-CSF–mediated, RT-induced, tumor-specific CTL responses.

In conclusion, our studies demonstrate that RT can change the immune profile of the tumor microenvironment and lead to the transient infiltration of antitumor RT-Ns into tumor tissue. Our studies further support the hypothesis that a combination of RT G-CSF enhances the tumor-specific adaptive immune response at both local and distal sites.

## Materials and Methods

A full discussion of experimental procedures is available in *SI Materials and Methods*.

**Animals.** Male C57BL/6 mice and female BALB/c mice, between 6 and 8 wk of age, were obtained from Taconic. All animal protocols were approved by the Institutional Animal Care and Use Committee of the University of Texas Southwestern Medical Center. This study was performed in strict accordance with the recommendations in the guidelines from the NIH.

**Cell Culture.** RM-9 prostate carcinoma was cultured in DMEM, and 4T1 mammary carcinoma and EG7 thymoma (EL4 transduced to express OVA) were cultured in RPMI-1640 supplemented with 10% (vol/vol) FCS, 2 mmol/L L-glutamine, 0.05 mmol/L 2-mercaptoethanol, Hepes, penicillin, and streptomycin. Cultures were maintained at 37 °C in a humidified atmosphere containing 5% $CO_2$.

**Local Irradiation.** The right leg with the target tumor was gently pulled out of the syringe hole, and the tumor was irradiated once with 15 Gy for RM-9 and 4T1 and with 1.3 Gy for EG7. Different tumors were given different doses according to their radiosensitivities (Fig. S1). Doses were delivered in a single fraction using a dedicated X-ray irradiator (X-RAD 320; Precision X-Ray, Inc.) with a 2-cm collimator. The device was operated at 250 kV and 1 mA, producing a dose rate of 1.27 Gy·$min^{-1}$.

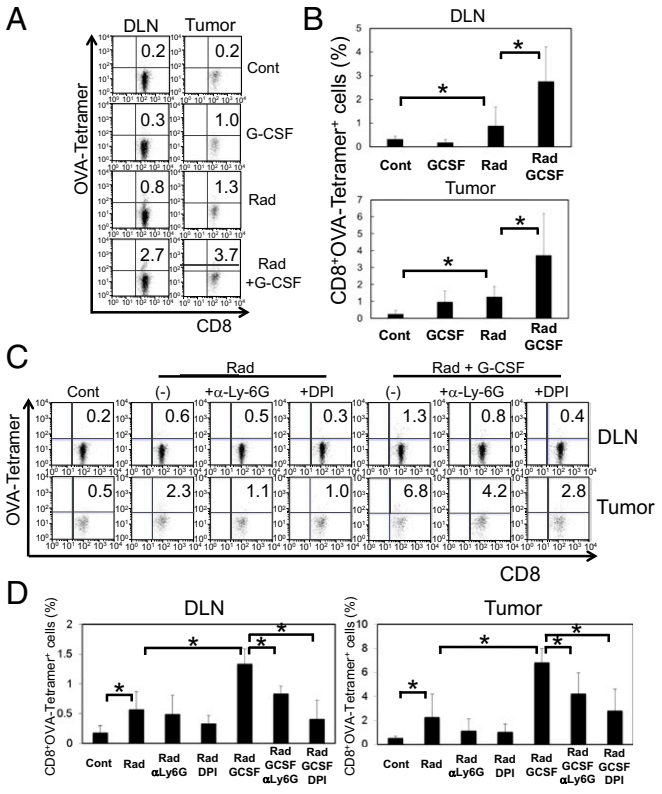


**Fig. 8.** G-CSF augments tumor-specific CTLs (OVA-$tetramer^+CD8^+$ cells) in DLNs and tumor tissues. Lymphocytes in both tissues were obtained from EG7-bearing mice 5 d after 1.3-Gy tumor irradiation either alone or in combination with anti–Ly-6G mAb, DPI, and G-CSF. G-CSF was injected s.c. for 4 consecutive days starting on the day of irradiation (*A–D*), anti–Ly-6G mAb was injected i.p. 1 d before irradiation (*C*), and DP was injected 5 min after irradiation (*D*). Analysis of differences was performed by the Mann–Whitney *U* test (*$P < 0.05$).

**Tumor RT Combined with G-CSF.** RM-9–, 4T1-, and EG7-bearing mice were irradiated as described above. Just after irradiation, G-CSF (150 μg/kg) was intradermally injected in proximity to the tumor. Injection of G-CSF was done four times each day. Antitumor activity was determined by measuring the tumor size in perpendicular diameters. Tumor volume was calculated in the manner described above.

**Statistical Analysis.** Data are presented as mean ± SEM. Analysis of differences was performed by the Mann–Whitney *U* test. For tumor growth studies comparing more than two groups, we used two-factor ANOVA with appropriate post hoc testing. Differences were considered significant when $P < 0.05$.

**ACKNOWLEDGMENTS.** We thank Dr. Hak Choy for funding and advice; Drs. Debabrata Saha, Michael Story, Hasan Zaki, Jeffrey Meyer, and Yang-Xin Fu for their advice; Dr. R. Thompson for providing the RM-9 cell line; Suneetha Eluru for her assistance on assays; and Dr. Damiana Chiavolini for editing our manuscript. We acknowledge the NIH Tetramer Core Facility (contract HHSN272201300006C) for providing the H-2$^{Kb}$ OVA-tetramer. We also thank the Flow Cytometry, Molecular Pathology, Animal Resource Center, and Genomics and Microarray Cores at the University of Texas Southwestern Medical Center. Research reported in this publication was supported by grants from the Department of Radiation Oncology, the University of Texas Southwestern Medical Center; the Cancer Immunobiology Center; the Simmons Patigian Chair; and the Horchow Foundation (E.S.V.).

1. Timmerman R, et al. (2010) Stereotactic body radiation therapy for inoperable early stage lung cancer. *JAMA* 303(11):1070–1076.
2. Demaria S, Golden EB, Formenti SC (2015) Role of local radiation therapy in cancer immunotherapy. *JAMA Oncol* 1(9):1325–1332.
3. Melief CJ (1992) Tumor eradication by adoptive transfer of cytotoxic T lymphocytes. *Adv Cancer Res* 58:143–175.
4. Houghton AM (2010) The paradox of tumor-associated neutrophils: Fueling tumor growth with cytotoxic substances. *Cell Cycle* 9(9):1732–1737.
5. Piccard H, Muschel RJ, Opdenakker G (2012) On the dual roles and polarized phenotypes of neutrophils in tumor development and progression. *Crit Rev Oncol Hematol* 82(3):296–309.
6. Brandau S, Dumitru CA, Lang S (2013) Protumor and antitumor functions of neutrophil granulocytes. *Semin Immunopathol* 35(2):163–176.
7. Fridlender ZG, et al. (2009) Polarization of tumor-associated neutrophil phenotype by TGF-beta: "N1" versus "N2" TAN. *Cancer Cell* 16(3):183–194.
8. Jablonska J, Leschner S, Westphal K, Lienenklaus S, Weiss S (2010) Neutrophils responsive to endogenous IFN-beta regulate tumor angiogenesis and growth in a mouse tumor model. *J Clin Invest* 120(4):1151–1164.
9. Eruslanov EB, et al. (2014) Tumor-associated neutrophils stimulate T cell responses in early-stage human lung cancer. *J Clin Invest* 124(12):5466–5480.
10. Kono H, Rock KL (2008) How dying cells alert the immune system to danger. *Nat Rev Immunol* 8(4):279–289.
11. Kolaczkowska E, Kubes P (2013) Neutrophil recruitment and function in health and inflammation. *Nat Rev Immunol* 13(3):159–175.
12. Lorimore SA, Coates PJ, Scobie GE, Milne G, Wright EG (2001) Inflammatory-type responses after exposure to ionizing radiation in vivo: a mechanism for radiation-induced bystander effects? *Oncogene* 20(48):7085–7095.
13. Nakayama E, Shiratsuchi Y, Kobayashi Y, Nagata K (2011) The importance of infiltrating neutrophils in SDF-1 production leading to regeneration of the thymus after whole-body X-irradiation. *Cell Immunol* 268(1):24–28.
14. François A, Milliat F, Guipaud O, Benderitter M (2013) Inflammation and immunity in radiation damage to the gut mucosa. *BioMed Res Int* 2013:123241.
15. Zitvogel L, Kepp O, Kroemer G (2010) Decoding cell death signals in inflammation and immunity. *Cell* 140(6):798–804.
16. Huebener P, et al. (2015) The HMGB1/RAGE axis triggers neutrophil-mediated injury amplification following necrosis. *J Clin Invest* 125(2):539–550.
17. Sadik CD, Kim ND, Luster AD (2011) Neutrophils cascading their way to inflammation. *Trends Immunol* 32(10):452–460.
18. Sumida K, et al. (2012) Anti-IL-6 receptor mAb eliminates myeloid-derived suppressor cells and inhibits tumor growth by enhancing T-cell responses. *Eur J Immunol* 42(8): 2060–2072.
19. Daley JM, Thomay AA, Connolly MD, Reichner JS, Albina JE (2008) Use of Ly6G-specific monoclonal antibody to deplete neutrophils in mice. *J Leukoc Biol* 83(1):64–70.
20. Sim S, et al. (2005) NADPH oxidase-derived reactive oxygen species-mediated activation of ERK1/2 is required for apoptosis of human neutrophils induced by Entamoeba histolytica. *J Immunol* 174(7):4279–4288.
21. Bauernfeind F, et al. (2011) Cutting edge: Reactive oxygen species inhibitors block priming, but not activation, of the NLRP3 inflammasome. *J Immunol* 187(2):613–617.
22. Roots R, Okada S (1975) Estimation of life times and diffusion distances of radicals involved in x-ray-induced DNA strand breaks of killing of mammalian cells. *Radiat Res* 64(2):306–320.
23. Mikkelsen RB, Wardman P (2003) Biological chemistry of reactive oxygen and nitrogen and radiation-induced signal transduction mechanisms. *Oncogene* 22(37):5734–5754.
24. Inoue Y, et al. (2014) NLRP3 regulates neutrophil functions and contributes to hepatic ischemia-reperfusion injury independently of inflammasomes. *J Immunol* 192(9):4342–4351.
25. Rothe G, Oser A, Valet G (1988) Dihydrorhodamine 123: A new flow cytometric indicator for respiratory burst activity in neutrophil granulocytes. *Naturwissenschaften* 75(7):354–355.
26. Lugade AA, et al. (2005) Local radiation therapy of B16 melanoma tumors increases the generation of tumor antigen-specific effector cells that traffic to the tumor. *J Immunol* 174(12):7516–7523.
27. Schaue D, et al. (2008) T-cell responses to survivin in cancer patients undergoing radiation therapy. *Clin Cancer Res* 14(15):4883–4890.
28. Lee Y, et al. (2009) Therapeutic effects of ablative radiation on local tumor require CD8+ T cells: Changing strategies for cancer treatment. *Blood* 114(3):589–595.
29. Takeshima T, et al. (2010) Local radiation therapy inhibits tumor growth through the generation of tumor-specific CTL: Its potentiation by combination with Th1 cell therapy. *Cancer Res* 70(7):2697–2706.
30. Apetoh L, et al. (2007) The interaction between HMGB1 and TLR4 dictates the outcome of anticancer chemotherapy and radiotherapy. *Immunol Rev* 220:47–59.
31. Marabelle A, Filatenkov A, Sagiv-Barfi I, Kohrt H (2015) Radiotherapy and toll-like receptor agonists. *Semin Radiat Oncol* 25(1):34–39.
32. Jablonska J, Wu CF, Andzinski L, Leschner S, Weiss S (2014) CXCR2-mediated tumor-associated neutrophil recruitment is regulated by IFN-β. *Int J Cancer* 134(6):1346–1358.
33. Andzinski L, et al. (2016) Type I IFNs induce anti-tumor polarization of tumor associated neutrophils in mice and human. *Int J Cancer* 138(8):1982–1993.
34. Mishalian I, et al. (2013) Tumor-associated neutrophils (TAN) develop pro-tumorigenic properties during tumor progression. *Cancer Immunol Immunother* 62(11):1745–1756.
35. Håkansson L, et al. (1997) Effects of in vivo administration of G-CSF on neutrophil and eosinophil adhesion. *Br J Haematol* 98(3):603–611.
36. Demers M, et al. (2012) Cancers predispose neutrophils to release extracellular DNA traps that contribute to cancer-associated thrombosis. *Proc Natl Acad Sci USA* 109(32):13076–13081.
37. Löwenberg B, et al.; Dutch-Belgian Hemato-Oncology Cooperative Group; Swiss Group for Clinical Cancer Research (2003) Effect of priming with granulocyte colony-stimulating factor on the outcome of chemotherapy for acute myeloid leukemia. *N Engl J Med* 349(8):743–752.
38. Bottoni U, et al. (2005) Complete remission of brain metastases in three patients with stage IV melanoma treated with BOLD and G-CSF. *Jpn J Clin Oncol* 35(9):507–513.
39. Staar S, et al. (2001) Intensified hyperfractionated accelerated radiotherapy limits the additional benefit of simultaneous chemotherapy–Results of a multicentric randomized German trial in advanced head-and-neck cancer. *Int J Radiat Oncol Biol Phys* 50(5):1161–1171.
40. Voloshin T, et al. (2011) G-CSF supplementation with chemotherapy can promote revascularization and subsequent tumor regrowth: Prevention by a CXCR4 antagonist. *Blood* 118(12):3426–3435.
41. Sheikh H, et al. (2011) Use of G-CSF during concurrent chemotherapy and thoracic radiotherapy in patients with limited-stage small-cell lung cancer safety data from a phase II trial. *Lung Cancer* 74(1):75–79.
42. Okazaki T, et al. (2006) Granulocyte colony-stimulating factor promotes tumor angiogenesis via increasing circulating endothelial progenitor cells and Gr1+CD11b+ cells in cancer animal models. *Int Immunol* 18(1):1–9.
43. Shojaei F, et al. (2009) G-CSF-initiated myeloid cell mobilization and angiogenesis mediate tumor refractoriness to anti-VEGF therapy in mouse models. *Proc Natl Acad Sci USA* 106(16):6742–6747.
44. Kim JS, et al. (2015) Administration of granulocyte colony-stimulating factor with radiotherapy promotes tumor growth by stimulating vascularization in tumor-bearing mice. *Oncol Rep* 34(1):147–154.
45. Belletti B, et al. (2008) Targeted intraoperative radiotherapy impairs the stimulation of breast cancer cell proliferation and invasion caused by surgical wounding. *Clin Cancer Res* 14(5):1325–1332.
46. Hannan R, et al. (2012) Combined immunotherapy with Listeria monocytogenes-based PSA vaccine and radiation therapy leads to a therapeutic response in a murine model of prostate cancer. *Cancer Immunol Immunother* 61(12):2227–2238.
47. Alfaro C, et al. (2011) Dendritic cells take up and present antigens from viable and apoptotic polymorphonuclear leukocytes. *PLoS One* 6(12):e29300.
48. Singhal S, et al. (2016) Origin and role of a subset of tumor-associated neutrophils with antigen-presenting cell features in early-stage human lung cancer. *Cancer Cell* 30(1):120–135.
49. Lim K, et al. (2015) Neutrophil trails guide influenza-specific CD8$^+$ T cells in the airways. *Science* 349(6252):aaa4352.
50. Pidikiti R, et al. (2011) Dosimetric characterization of an image-guided stereotactic small animal irradiator. *Phys Med Biol* 56(8):2585–2599.
51. Shehan DC, Hrapchak BB (1980) *Theory and Practice of Histotechnology* (Battelle Press, Columbus, OH), 2nd Ed.
52. Woods AE, Ellis RC (1996) *Laboratory Histopathology, A Complete Reference* (Churchill Livingstone, London).